Neuro-Oncology
24(5), 694–707, 2022 | https://doi.org/10.1093/neuonc/noab244 | Advance Access date 17 October 2021

Anti-invasive efficacy and survival benefit of the YAP-TEAD inhibitor Verteporfin in preclinical glioblastoma models

Anne Marie Barrette, Halle Ronk, Tanvi Joshi, Zarmeen Mussa, Meenakshi Mehrotra, Alexandros Bouras, German Nudelman, Joe Gerald Jesu Raj, Dominique Bozec, William Lam, Jane Houldsworth, Raymund Yong, Elena Zaslavsky, Constantinos G. Hadjipanayis, Marc R. Birtwistle, and Nadejda M. Tsankova

Department of Pathology, Icahn School of Medicine at Mount Sinai, New York, New York, USA (A.M.B., H.R., T.J., Z.M., M.M., W.L., J.H., N.M.T.); Department of Neurosurgery, Icahn School of Medicine at Mount Sinai, New York, New York, USA (A.B., J.G.J.R., D.B., R.Y., C.G.H.); Department of Neurology, Icahn School of Medicine at Mount Sinai, New York, New York, USA (G.N., E.Z.); Department of Neuroscience, Icahn School of Medicine at Mount Sinai, New York, New York, USA (N.M.T.); Department of Neurosurgery, Stanford University, Stanford, California, USA (A.M.B.); Department of Chemical and Biomolecular Engineering, Clemson University, Clemson, South Carolina, USA (M.R.B.)

Corresponding Author: Nadejda Tsankova, MD, PhD, Department of Pathology, Icahn School of Medicine at Mount Sinai, 1425 Madison Avenue, New York, NY 10029, USA (nadejda.tsankova@mssm.edu).

Abstract

Background. Glioblastoma (GBM) remains a largely incurable disease as current therapy fails to target the invasive nature of glioma growth in disease progression and recurrence. Here, we use the FDA-approved drug and small molecule Hippo inhibitor Verteporfin (VP) to target YAP-TEAD activity, known to mediate convergent aspects of tumor invasion/metastasis, and assess the drug's efficacy and survival benefit in GBM models.

Methods. Up to 8 low-passage patient-derived GBM cell lines with distinct genomic drivers, including 3 primary/recurrent pairs, were treated with VP or vehicle (VEH) to assess in vitro effects on proliferation, migration, invasion, YAP-TEAD activity, and transcriptomics. Patient-derived orthotopic xenograft (PDX) models were used to assess VP's brain penetrance and effects on tumor burden and survival.

Results. VP treatment disturbed YAP/TAZ-TEAD activity; disrupted transcriptome signatures related to invasion, epithelial-to-mesenchymal, and proneural-to-mesenchymal transition, phenocopying TEAD1-knockout effects; and impaired tumor migration/invasion dynamics across primary and recurrent GBM lines. In an aggressive orthotopic PDX GBM model, short-term VP treatment consistently diminished core and infiltrative tumor burden, which was associated with decreased tumor expression of Ki67, nuclear YAP, TEAD1, and TEAD-associated targets EGFR, CDH2, and ITGB1. Finally, long-term VP treatment appeared nontoxic and conferred survival benefit compared to VEH in 2 PDX models: as monotherapy in primary (de novo) GBM and in combination with Temozolomide chemoradiation in recurrent GBM, where VP treatment associated with increased *MGMT* methylation.

Conclusions. We demonstrate combined anti-invasive and anti-proliferative efficacy for VP with survival benefit in preclinical GBM models, indicating potential therapeutic value of this already FDA-approved drug if repurposed for GBM patients.

Key Points

- The YAP-TEAD inhibitor Verteporfin disrupts migration/invasion dynamics across GBM types.
- Short-term drug treatment diminishes infiltrative tumor growth in aggressive PDX.
- This FDA-approved drug confers survival benefit in PDX models.

Importance of the Study

Glioblastoma (GBM) remains an incurable disease, in large part due to the lack of therapy against its malignant infiltrative spread. Here, we used the YAP-TEAD inhibitor Verteporfin (VP) to target a convergence point for regulating tumor invasion/metastasis. VP is known to diminish GBM growth but its anti-invasive efficacy in orthotopic models is not well established. Our results indicate a novel role for VP beyond inhibiting proliferation, demonstrating a robust impact of this drug on the dynamics of tumor migration, invasion, and mesenchymal transition across different IDH-wildtype GBM lines. Notably, our study also provides the first survival efficacy data for VP in primary and recurrent preclinical GBM models, demonstrating survival benefit of the drug at nontoxic doses. These results encourage consideration for repurposing the FDA-approved drug VP for treatment in GBM patients with primary and/or recurrent disease.

Glioblastoma (GBM) is characterized by rapid growth within a densely cellular and proliferative tumor core and expansile, diffusely infiltrative periphery with distinct microenvironment and molecular signature.[1–4] The tumor core contains the defining histopathological features of GBM, is represented in most tissue biopsies, better understood biologically, relatively more drug-penetrant, and partially responsive to anti-proliferative therapy. Thus, it is a prime target in many therapeutic efforts. In recent years, however, it has become clear that glioma cells within the infiltrative margin are largely responsible for tumor recurrence, by evading both surgical treatment and chemoradiation, highlighting the need for better understanding of migratory GBM biology and improved combination therapy that targets not only proliferation but also the infiltrative tendency of glioma cells.[2,5]

Recent studies have described tumor migration as an adaptive phenotype in a subpopulation of therapy-resistant glioma cells with cancer stem cell properties, also referred to as glioma stem cells (GSCs),[6,7] and our group uncovered TEAD1 as an important regulator of tumor cell migration in GSCs.[8] The TEAD family of transcription factors (TFs), along with their coactivators YAP/TAZ, are the main downstream effectors of the Hippo pathway. Hippo controls organ size during development and integrates complex chemical, cytoskeletal, and mechanical microenvironmental cues related to cell movement, which converge on the nuclear translocation of YAP or its paralog TAZ, and ultimately on YAP/TAZ-TEAD-mediated transcription. The role of Hippo dysregulation in tumor invasion, metastasis, and epithelial-mesenchymal transition (EMT) is well established in several cancer types outside of the neuraxis.[9] In gliomas, overexpression of both YAP and TAZ correlates with higher tumor grade and worse prognosis[10,11] and aberrant Hippo-YAP-TEAD signaling has been implicated in GBM growth, invasion, and mesenchymal differentiation.[10–18] Yet, the therapeutic efficacy of Hippo pathway inhibitors in GBM remains largely unexplored.

Verteporfin (VP) (distinct liposomal formulation under the brand name Visudyne®), a long-time FDA-approved drug for macular degeneration, was recently discovered to act as a small molecule inhibitor of YAP-TEAD[19] and TAZ-TEAD[9,20] activity and has been subsequently shown to have anti-cancer efficacy in several solid tumor types.[19,21–23] Recent GBM studies have shown that VP decreases proliferation and induces glioma cell death in vitro,[24–27] and attenuates tumor growth in subcutaneous xenografts[28] and in an EGFR-mutant mouse model.[29] However, the drug's efficacy across GBM subtypes, and its anti-invasive properties, remain unexplored. Here, we use transcriptomics and functional assays to characterize a broad inhibitory effect of VP on GBM cell migration/invasion and mesenchymal transition, and then perform translational studies with this YAP-TEAD inhibitor in preclinical GBM mouse models, demonstrating consistent anti-invasive efficacy and a survival benefit of VP at nontoxic levels in patient-derived orthotopic xenograft (PDX) tumors.

Methods

Samples

Samples were collected, de-identified, and processed in accordance with the policies and regulations at Icahn School of Medicine at Mount Sinai (ISMMS) and its institutional review board. Experiments were performed on 8 distinct patient-derived IDH-wildtype GBM cell lines at low passage[8,30] treated with VP (MedChemExpress), Erlotinib (ERL) (SelleckChem), or equivalent DMSO vehicle (VEH). For all experiments, only cells attached to the plate were used for downstream experiments after visual inspection to confirm their intact cytoplasm and lack of apoptosis or crenation; non-detached dead/dying cells were removed.

Migration, Invasion, Viability, and Proliferation Assays

Cell viability and proliferation experiments were performed in serum-free conditions at low density (2500 cells per well), using Hoechst and Draq7 staining to determine total and dead cell count, respectively, and using MTT assays. Drug doses (IC25/50/75) were calculated based on 72 h of VP treatment. Migratory behavior was assessed by spheroid dispersion/migration at 36 h of drug treatment and by transwell invasion assays (viable cell fraction only), as previously described.[8] Sphere viability was assayed using the Cell Titer Blue assay (Promega, G808A). Growth factors (EGF, bFGF) were omitted in spheroid migration, Hoechst/DRAQ7 death/proliferation, Cell Titer Blue viability, and transwell invasion assays, and in cells grown for immunohistochemistry and RNA-seq analyses.

Transcriptome (RNA-Seq) Analysis

RNA was extracted from the viable cell fraction of drug/VEH-treated cells (RNeasy, Qiagen) to generate cDNA libraries (Takara 634874). RNA-seq was performed on Illumina HiSeq 2500 (50 bp paired-end) with downstream quality control, alignment (GENCODE GRCh38), data normalization, and differential expression analyses as recently described.[8] Expression of selected genes was validated by qRT-PCR.

MGMT Methylation

DNA methylation at *MGMT* was assessed in each cell line and G-16302 PDX tumors using a clinically validated in-house assay. DNA was extracted (Maxwell 16, Promega AS1130), bisulfite-converted, and subjected to pyrosequencing at CpG sites 74-78 of *MGMT* exon 1 using human-specific primers (PyroMark Q24, Qiagen 970032). Results were corroborated in a subsequent, independent experiment.

Orthotopic Transplantations and Drug/Radiation Animal Treatments

Animal studies were performed in accordance with the ethical standards of ISMMS under approved Institutional Animal Care and Use Committee protocols. Patient-derived G-16302 (2×10^5) and G-13063 (5×10^5) cells were injected stereotactically into the striatum (2 mm right lateral to bregma and 3 mm deep) of 2-month-old male and female mice with B&T-cell immunodeficiency but retained microglia activity (IcrTac:ICR-PrkdcSCID strain, Taconic). VP (reconstituted in DMSO) or VEH (equivalent DMSO concentration) were administered intraperitoneally (IP) daily (6 mg/kg, 10 mg/kg, and 100 mg/kg doses) or every other day (50 mg/kg dose). Temozolomide (TMZ, 5 mg/kg IP) and whole-brain radiation therapy (RT, 3Gy) were administered on 2 consecutive days. All treatments were randomized. Mice were sacrificed for histological analysis of tumor burden or for survival studies when clinically symptomatic or reaching 20% weight loss from time of transplantation.

IVIS Imaging

IVIS spectrum in vivo imaging (PerkinElmer) was used to measure VP's natural light-induced fluorescence (excitation = 605 nM, emission = 700 nM) in anesthetized mice, ~2 hours (h) and ~24-h post-VEH (DMSO) or VP (6 mg/kg, 10 mg/kg, or 50 mg/kg) IP injection. IVIS measurements were set to predefined tissue depth and regions of interest of equal size and shape were applied to capture total flux (photons per second). Image acquisition and analysis were performed using LivingImage.

Immunofluorescence

Immunofluorescence was performed as previously described,[31] on 4% PFA 2-dimensional cultures and PDX cryosections, using the following primary antibodies: TEAD1 (BD610923, 1:100), EGFR (Invitrogen 280005, 1:100; Millipore 06-847, 1:100), Ki67 (Abcam ab15580, 1:250), YAP (Cell Signaling 4912, 1:200), TAZ (Abcam ab84927, 1:200), CDH2 (BD610921, 1:100), ITGB1 (ABclonal A2217, 1:100), cleaved Caspase-3 (Cell Signaling 9661, 1:200), and human nuclear antigen (HNA) (Millipore MAB1281, 1:400); counterstained with DAPI (Thermo Fisher D1306, 1:1000). Images were captured on Zeiss LSM 710 confocal microscope or IN Cell Analyzer and quantitated under uniform gain settings using Zen 2 Blue or ImageJ. Only cultured cells with viable appearance were scored.

Statistical Analysis

Student *t* test and 1- or 2-way ANOVA were used, as appropriate, to calculate significance (*$P < .05$, **$P < .01$, ***$P < .001$) in cell culture and imaging studies. RNA-seq

Table 1 GBM Cell Line Information

GBM Cell Line	Primary/Recurrent	Patient Sex	*IDH* Status	*PDGFRA* Amplification	*NF1* Mutation	*PTEN* Mutation	*TP53* Mutation	*EGFR* Mutation/CNA	*MGMT* Methylation (%)
G-13063	Primary	Female	wt	✓	✓				52.4
G-12746	Primary	Male	wt				✓	✓	92.2
G-13181	Primary	Female	wt		✓				39.6
G-16302	Recurrent	Female	wt		✓				37.1
G-13514	Primary	Female	wt					✓	96.2
G-17969	Recurrent	Female	wt					✓	93
G-11849	Primary	Female	wt	✓		✓			58.2
G-11849R	Recurrent	Female	wt	✓		✓			86.6
U87	Established	Male	wt			✓			

Provided is information on experimental cells used—8 patient-derived lines at low passage (<30) (G-13063, G-12746, G-13181, G-16302, G-13514, G-17969, G-11849, G-11849R) and U87 GBM cell line, patient sex, primary/recurrent status, main genomic alterations of original tumor; and patient-derived cell line MGMT DNA methylation levels. All 8 patient-derived lines were used for functional in vitro experiments; G-13063 and G-16302 lines were used for in vivo experiments; G-13063, G-16302, and U87 cells were used for RNA-seq experiments. **Abbreviation:** CNA, copy number alteration.

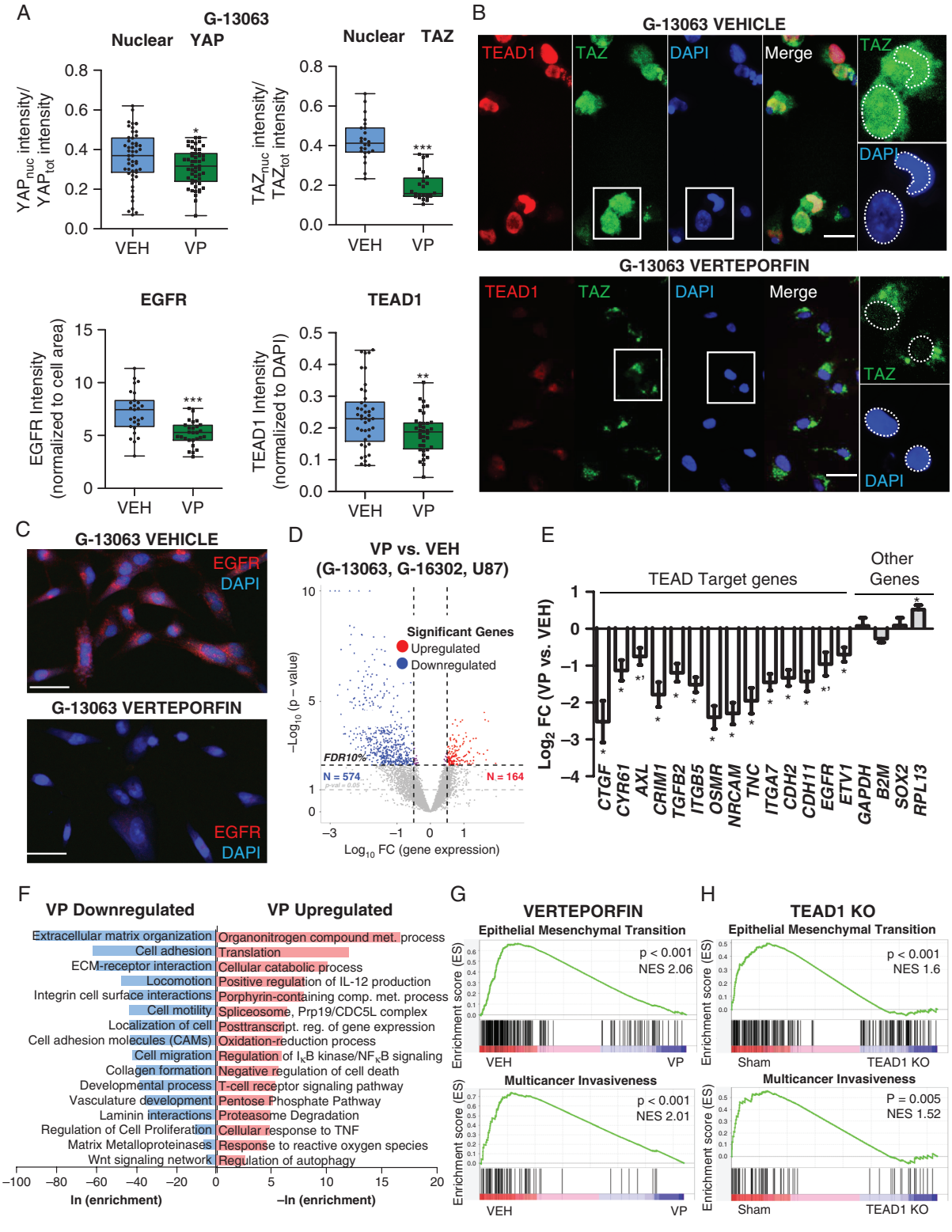

Fig. 1 Verteporfin downregulates YAP/TAZ-TEAD activity and transcriptomes related to adhesion, EMT, and invasion in GBM. (A) Immunocytochemistry analysis of subcellular expression of TAZ, YAP, TEAD1, and the TEAD1-target EGFR after 3-day treatment with Verteporfin (VP) (IC_{50} dose) vs vehicle (VEH) in G-13063 cells; *P = .017 (YAP), ***P = .0001 (TAZ), **P = 0.0046 (TEAD1), ***P = .00001 (EGFR) by Student t test; n = 24-51 images (dots) in 2-5 wells/condition; lines in box-and-whisker plots represent mean and bars represent min/max. See also Supplementary Figure 2. (B) Representative images of TAZ and TEAD1 from part A. Scale bars = 25 μm. (C) Representative images of EGFR from part A. Scale bars = 50 μm. (D) Volcano plot of differential expression RNA-seq data from 3 biologically distinct GBM lines (G-13063, G-16302, U87)

differential expression tests were false discovery rate (FDR)-adjusted for multiple testing correction. IC_{50} values were calculated as a function of 7 different log-fold concentrations. The chi-square log-rank test was used to calculate significance in Kaplan-Meier survival analyses (*$P < .05$).

Results

Verteporfin Inhibits YAP/TAZ-TEAD Activity and Disrupts Invasion and Pro-Mesenchymal Transcriptome Signatures

Hippo dysregulation has been recently implicated in GBM invasion and migration.[13–17] To explore the efficacy of the small molecule Hippo-YAP/TAZ-TEAD inhibitor VP in this context, we first tested drug activity in 8 biologically distinct patient-derived GBM cell lines with unique genomic alterations, including 3 primary/recurrent pairs (Table 1). Cell viability and IC_{50} dose was determined for each line, following 3 days of drug treatment (Supplementary Figure 1A), revealing overall similar sensitivity of cell lines to VP treatment, despite unique genomic makeup and primary vs recurrent status. In these, VP treatment downregulated protein expression of key Hippo pathway members YAP/TAZ and inhibited TEAD1 activity (Figure 1A–C, Supplementary Figure 2A–E), as seen with other cancers.[19,21–23] Notably, the decrease in YAP and TAZ expression was specific to the nucleus (Figure 1A and B, Supplementary Figure 2A–C), consistent with the known effect of VP on cytoplasmic YAP/TAZ sequestration.[32] Controlled time-course analysis of cell death after VP treatment indicated slow and gradual increase in dying cells over the 72-h period, negligible before 36 h (Supplementary Figure 1B and C). Of note, cell death did not differ significantly between light-on and light-off conditions during VP administration (Supplementary Figure 1B), and there was a persistent decrease in nuclear YAP and EGFR levels within the live cell fraction of treated cells (Supplementary Figure 2E).

To assess VP's effect on YAP/TAZ-TEAD transcriptional activity and on overall tumor biology genome-wide, we performed whole transcriptome RNA-seq on viable GBM cells with distinct phenotypes (Table 1), treated with VP, VEH, or the drug ERL to control for nonspecific drug effects (Supplementary Data 1). Unsupervised hierarchical clustering and differential expression analysis of VP vs VEH treatment defined robust VP-associated signature in all biological replicates, despite strong patient-specific separation (Figure 1D, Supplementary Figure 3A–C), whereas the same analysis for ERL vs VEH treatment did not (Supplementary Figure 3A and B, Supplementary Data 1). We confirmed significant downregulation of many known YAP/TAZ-TEAD-target genes across all cell lines after VP treatment, including *CTGF* (*CCN2*), *Cyr61* (*CCN1*), *TGFB2*, *ITGB5*, *AXL*, and *EGFR*[8,9,22,23] (Figure 1E, Supplementary Figure 2F), and validated several of them orthogonally (Figure 1A and C; Supplementary Figure 2D and G). Functional enrichment analyses revealed most significant enrichment for biological processes and pathways related to extracellular matrix (ECM) organization, adhesion, EMT, migration, locomotion, and cell motility in the downregulated set of genes after VP treatment (Figure 1F, Supplementary Figure 3D, Supplementary Data 1). Processes related to cell proliferation were also represented by a few genes, with much lower enrichment significance (Figure 1F). In contrast, upregulated genes after VP treatment were highly enriched for pathways related to nitrogen and porphyrin-related metabolism and translational initiation (Figure 1F, Supplementary Figure 3D).

To define better the on- vs off-target effects of VP as a TEAD inhibitor, we compared enrichment of gene set signatures in VP-treated cells to similar patient-derived cell lines in which TEAD1 was ablated using CRISPR/Cas9 genomic editing (TEAD1 knockout).[8] Notably, this analysis disclosed similar effect on the enrichment of mesenchymal (EMT), invasiveness,[33] and proneural-to-mesenchymal (PMT)/multitherapy resistance[34] signatures between VP treatment and TEAD1 knockout conditions (Figure 1G and H, Supplementary Figure 4A and B, Supplementary Data 1) while also revealing some transcriptome differences (Supplementary Figure 4C and D). Overall, the transcriptome analysis suggested that VP treatment overwhelmingly inhibits invasion, ECM organization, and pro-mesenchymal EMT and PMT pathways across distinct GBM subtypes, substantiating further studies to assess the drug's anti-invasive therapeutic efficacy.

Verteporfin Impairs Glioblastoma Migration and Invasion Dynamics In Vitro

VP is known to decrease proliferation and induce glioma cell death in vitro.[24–27] Here, we tested if pharmacological inhibition of YAP/TAZ-TEAD activity also has a functional effect on GBM migration and invasion in our patient-derived cell line models, using the spheroid dispersal/confluent migration and transwell invasion assays. To minimize the confounding effects of cell proliferation and cell death on tumor migration, spheroid dispersal assays were performed in the absence of growth factors, over an early 36-h time course when anti-proliferative VP

Fig. 1, continued
treated with VP (IC_{50} dose) vs VEH for 3 days. Defined set of 574 downregulated and 164 upregulated genes are marked by blue and red dots, respectively (10% false discovery rate [FDR] adjustment). (E) TEAD-target gene expression in the differential RNA-seq dataset from (D) (*$P < .05$ and *'$P < .1$ by Student *t* test; n = 3 cell lines; bars represent mean ± SEM). (F) Functional enrichment analysis on the differential sets of genes from part (D) (log_2-fold change >0.5 and <-0.5) against several gene set databases, HOMER tool. Shown are selected top enriched biological processes, pathways, and reactomes of downregulated (blue) or upregulated (red) VP-associated genes (see Supplementary Data 1 for full list). (G) Gene Set Enrichment Analysis (GSEA) of the predefined signature gene sets "HALLMARK EPITHELIAL MESENCHYMAL TRANSITION" (M5930) and "Multicancer Invasiveness"[33] in the VP/VEH rld normalized RNA-seq dataset. (H) GSEA analysis of rld normalized RNA-seq dataset from CRISPR/Cas9 TEAD1 knockout cell lines vs sham (G-13063, G-16302, G-12746, and G-13306 cell lines[8]), phenocopying the enrichment pattern seen in VP-treated cells. Abbreviations: EMT, epithelial-mesenchymal transition; GBM, glioblastoma; NES, normalized enrichment score.

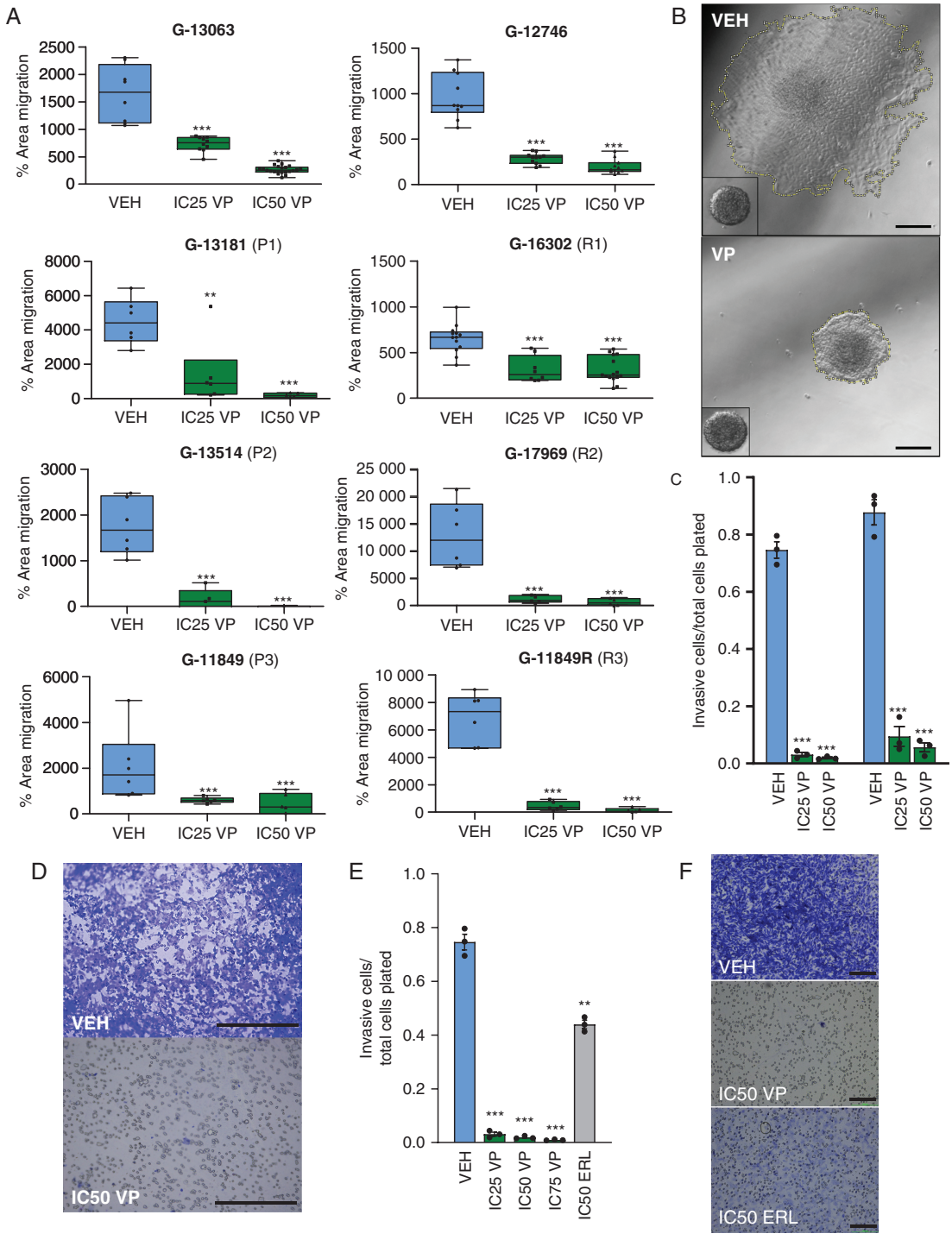

Fig. 2 Verteporfin decreases tumor migration in vitro across primary and recurrent GBMs. (A) Dose-dependent effect of Verteporfin on spheroid dispersion/confluent cell migration, across 8 biologically distinct GBM lines, including 3 primary (P1-P3) and recurrent (R1-R3) pairs (n = 3 wells (dots) with multiple spheres/well, 2 independent experiments for G-13063 and G-16302; lines in box and whisker plots represent the mean spheroid area at 36 h after treatment, bars represent min/max). (B) Area of spheroid migration in representative G-13063 cells at 36 h of treatment with VEH or IC50 VP, marked by yellow dash line; inset shows spheroid at 1 h. Scale bars = 75 μm. (C) Dose-dependent effect of Verteporfin on transwell invasion. Dead cells are discarded prior to transwell plating and live cell number is measured using crystal violet (n = 3 wells (dots) per condition for each line). (D) Representative images of transwell membranes were analyzed in (C). Scale bars = 50 μm. (E) Identical transwell invasion assays to part (C) comparing effect of invasion in G-13063 cells treated with VEH, VP, or ERL (n = 3 wells (dots) per condition). (F) Representative images of transwell membranes from (E). Scale bars = 100 μm. (*$P < .05$, **$P < .01$, ***$P < .001$ by Student t test; dose-dependence confirmed by ANOVA ($P < .05$); C, E: bars represent mean ± SEM). Abbreviations: ERL, Erlotinib; GBM, glioblastoma; VEH, vehicle; VP, Verteporfin.

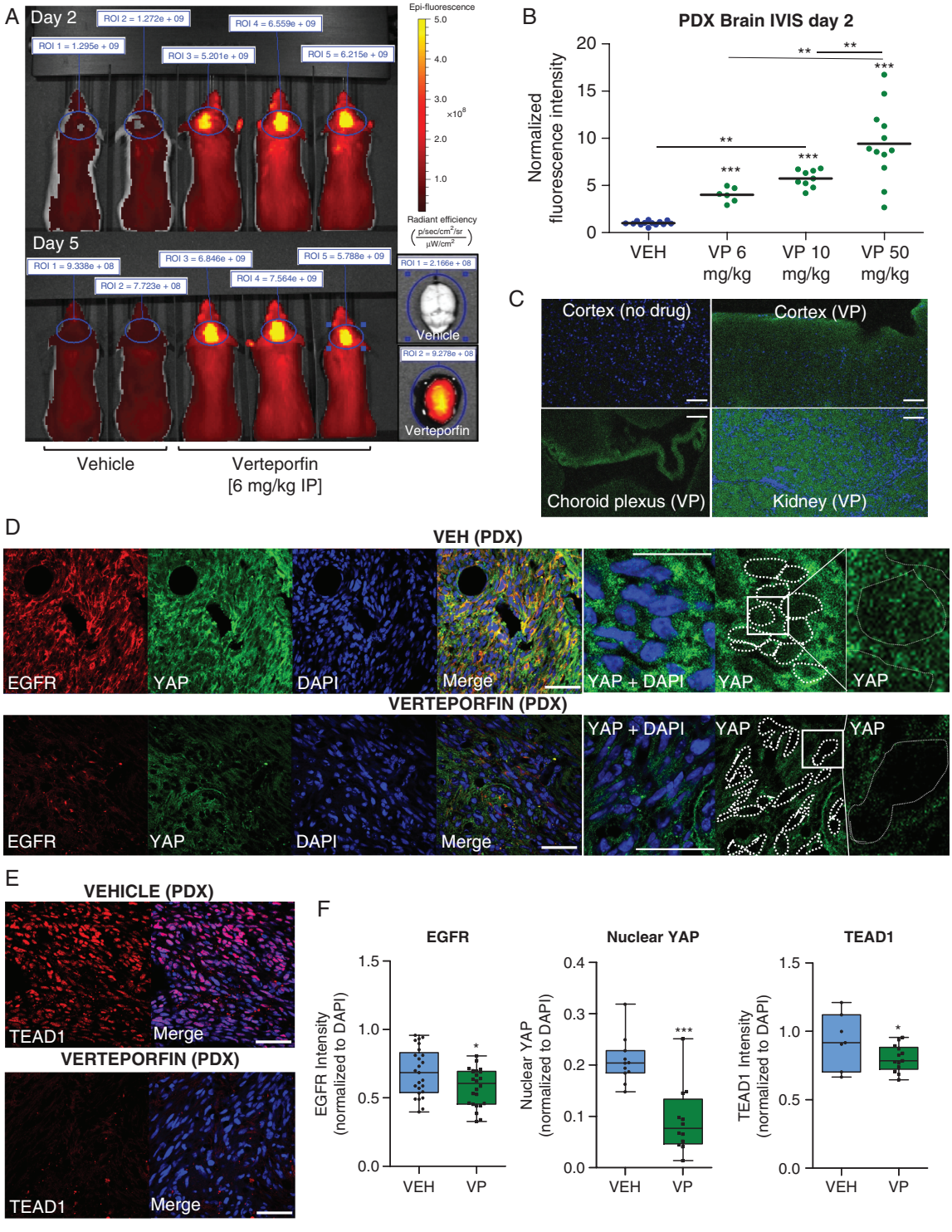

Fig. 3 Brain accumulation and YAP-TEAD activity of Verteporfin in PDX tumors. (A) IVIS imaging in anesthetized littermate G-16302 PDX mice 2 h after VP administration on days 2 and 5 (6 mg/kg IP), measured at 605 nm/700 nm excitation/emission. On right, brain organ fluorescence at necropsy 2.5 h after treatment, day 5. Regions of interest (ROI) for intensity measurements are marked by blue lines. (B) Dose-dependent accumulation of VP-associated fluorescence in G-16302 PDX brains, normalized IVIS data over multiple experiments; ***$P < .0001$ (VEH) vs 6 mg/kg/10 mg/kg/50 mg/kg (VP); **$P = .0011$ 6 mg/kg (VP) vs 10 mg/kg (VP); **$P = .0069$ 10 mg/kg (VP) vs 50 mg/kg (VP) by Student t test; dose-dependence also significant by 1-way ANOVA, $P < .0001$; n = 13 (VEH), 6 (6 mg/kg VP), 9 (10 mg/kg VP),12 (50 mg/kg VP) PDX mice (dots); lines in plot represent mean. All IVIS measurements are performed using identical settings on day 2 of treatment, ~2 h after drug administration. (C) Accumulation of VP-associated autofluorescence (green) throughout the brain parenchyma, including outside cerebral vessels, assessed by epifluorescence microscopy (kidney shown as positive control and choroid plexus shows relative accumulation in vasculature (10 mg/kg intravenous VP, 2 h). Scale

effects were found to be non-significant (Supplementary Figure 1D, E, and F) and the rate of cell death was low (Supplementary Figure 1B and C), using lower and higher doses of VP.[8,35,36] Treatment with VP resulted in significant, dose-dependent decrease in confluent cell migration across all 8 patient-derived GBM cell lines, both primary and recurrent subtypes (Figure 2A and B), as well as in robust, dose-dependent decrease in cell invasion within the viable fraction of treated cells (Figure 2C and D). Compared to treatment with the EGFR inhibitor ERL, the anti-invasion effect of VP was much more pronounced (Figure 2E and F). Overall, this analysis substantiated the anti-migration efficacy of VP across patient-derived GBM cell lines with distinct genomic drivers, both in primary and recurrent settings.

Brain Accumulation and Hippo Target Inhibition of Verteporfin in PDX Models

Structurally, VP is a benzoporphyrin-derived monoacid of small-to-medium size and distinctly lipophilic character[37] and has been shown to be brain penetrant without the need of a carrier.[29,38]To assess if VP reaches the brain parenchyma in our PDX models, we took advantage of the drug's intrinsic fluorescence and used IVIS imaging to demonstrate significant accumulation of VP-associated signal in the brain of live animals over the course of drug treatment as well as within their tissue organ at necropsy (Figure 3A, Supplementary Figure 5A). Importantly, the increase in VP-associated fluorescence was dose-dependent (Figure 3B) and persisted above VEH 24 h after drug administration (Supplementary Figure 5B). Microscopy analysis confirmed that VP-associated fluorescence is seen throughout the neuropil parenchyma and not just within blood vessels (Figure 3C). While the exact inhibitory concentration of VP could not be determined in vivo, we found that IP injection of VP for 10 days at nontoxic dose was sufficient to exert on-target activity, inhibiting nuclear YAP, TEAD1, and TEAD1-target expression in PDX tumors (Figure 3D–F).

Verteporfin Treatment Decreases Infiltrative Tumor Burden and Proliferation In Vivo

Encouraged by the consistent accumulation of VP signal and the drug's impact on YAP-TEAD expression in the brain, we set out to characterize the effect of short-term VP treatment on tumor growth and infiltrative spread. We used the aggressive G-16302 orthotopic PDX model, derived from a patient with a recurrent (therapy-resistant) and widely metastatic GBM,[30] which consistently shows the formation of large and diffusely infiltrative tumors by 4 weeks and clinical deterioration by 5-6 weeks. Mice with G-16302 PDX tumors were treated with VP (or VEH) for 1 week, beginning at 3-week post-xenotransplantation (pt). Tumor burden area at the core and at the infiltrative edge was annotated based on tumor cell density and measured on serial histological sections. This analysis revealed significantly lower tumor burden in VP-treated mice, both within the leading infiltrative tumor edge extending into the corpus callosum, as well as within the tumor's core, observed consistently across 3 independent experiments (Figure 4A, B, and G). A decrease in the distal migration of single tumor cells was also noted when PDX mice were treated with VP for 4 weeks (Figure 4G and H, Supplementary Figure 5F). Within the tumor core, VP treatment showed a subtle but significant inhibitory effect on cell proliferation (Figure 4C and D) and only a modest effect on cell apoptosis (Supplementary Figure 5C), the latter suggesting that the main effect of VP treatment in our model appears to be on live cell dynamics rather than on cell death. Probing further into VP's dynamic effects on tumor burden, we measured the expression of several VP-associated targets most strongly downregulated in the RNA-seq analysis (Supplementary Figure 3D, Supplementary Data 1) and found significant downregulation of the mesenchymal cadherin CDH2 and the integrin ITGB1 in VP-treated PDX tumors (Figure 4E and F, Supplementary Figure 5D and E). Importantly, downregulation of CDH2 and ITGB1 levels corresponded to lower nuclear YAP and TEAD1 expression (Figure 3D–F) and to reduced infiltrative tumor burden (Figure 4A, B, and G) in the same PDX tumors. Overall, these in vivo drug efficacy data provide strong evidence that VP diminishes infiltrative growth and spread in an aggressive, recurrent PDX model, and can even impede distal cell migration if given early on in the disease's course.

Verteporfin Confers Survival Benefit Without Systemic Toxicity in PDX Models

Translational efforts are urgently needed to bring forward new therapeutics against the invasive biology of GBM, responsible for tumor recurrence. To explore if VP's anti-invasive efficacy confers survival benefit in preclinical models, we administered VP or VEH daily, either as monotherapy or in combination with standard chemoradiation therapy (TMZ plus fractionated RT) in gender-matched mice with G-16302 PDX tumors. Treatment with VP (or VEH) began 2-week post-orthotopic xenotransplantation, and fractionated RT was administered with 2 doses of 3Gy after IP injection of TMZ 1 week later (Figure 5A). In this aggressive PDX model, we detected statistically significant survival difference only between mice treated with VP in combination with chemoradiation (VP + TMZ + RT) and mice given VEH (P = .02), with VP + TMZ + RT-treated mice

Fig. 3, continued
bars = 50 µm. (D, E) Representative immunofluorescence images of EGFR and YAP (D) and TEAD1 (E) expression in the core of G-16302 PDX tumors after VP treatment (100 mg/kg IP, 10 days). Scale bars = 50 µm. (F) Quantification of normalized intensity for TEAD1's target EGFR, nuclear YAP, and TEAD1 in tumor core, using single confocal plane images; *P = .01 (EGFR), *P = .03 (TEAD1), ***P < .0001 (nuclear YAP) by 1-tailed unpaired Student t test, n = 6 mice (EGFR) and n = 4 mice (TEAD1) with multiple fields scored; lines in box-and-whisker plots represent mean and bars represent min/max. Abbreviations: IP, intraperitoneally; PDX, patient-derived orthotopic xenograft; VEH, vehicle; VP, Verteporfin.

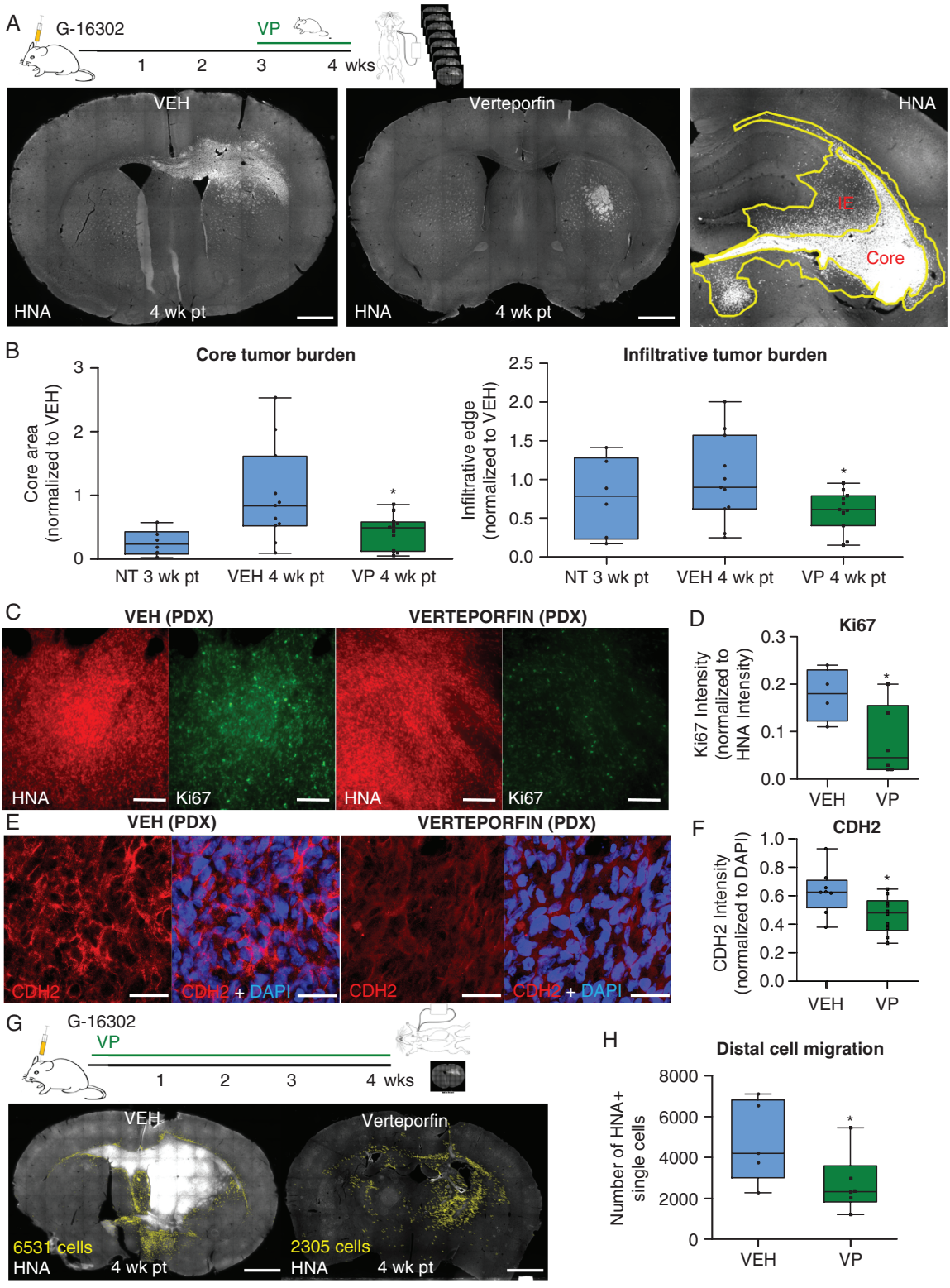

Fig. 4 Verteporfin decreases infiltrative tumor burden in aggressive PDX tumors. (A) Experimental setup and representative histological sections of infiltrative G-16302 PDX tumors at 4-week post-transplantation (wk pt) treated with vehicle or Verteporfin (100 mg/kg IP, days 21-30). Tumors are stained with human nuclear antigen (HNA). "Core" is defined as tumor area near the injection site with highest tumor density (>100 HNA+/HNA– cells) and "infiltrative edge" (IE) is defined as adjacent tumor area of lower tumor density (~50-100 HNA+/HNA– cells) and confluent tumor spread, marked by yellow lines. Scale bar = 1 mm. (B) Quantification of PDX tumor burden area within the tumor "core" and "infiltrative edge" in 8

showing 16.5 days longer median survival compared to VEH-treated mice (Figure 5A). Statistically significant survival benefit was not detected with VP treatment alone and with chemoradiation (TMZ + RT) treatment alone, consistent with the treatment-resistant nature of the recurrent G-16302 GBM model.[30] Survival analysis of VP + TMZ + RT vs TMZ + RT was also not significant (P = .2), although a transient pro-survival effect was observed when VP was added to TMZ + RT (Figure 5A). Importantly, VP administration over several different doses (6-100 mg/kg IP) for up to 39 days did not show any evidence for systemic toxicity prior to tumor formation, based on frequent monitoring for weight loss, signs of clinical deterioration, and confirmation of tumor formation at necropsy. To study further the basis for the longer survival observed in some of the mice treated with VP in combination with chemoradiation, we performed additional histological analyses and measured levels of *MGMT* methylation in the survival G-16302 PDX cohort. Interestingly, molecular analysis revealed statistically significant increase in human *MGMT* methylation levels in VP-treated PDX tumors, both in the VP alone and the VP + TMZ + RT combination groups (Figure 5B), pointing toward a VP-associated effect on *MGMT* methylation. Histologically, tumors appeared large and infiltrative at end stage, with VP and VP + TMZ + RT treatment showing significantly lower tumor density compared to TMZ + RT treatment (Supplementary Figure 6A–C). Tumors treated with RT also displayed treatment-related necrosis, which, notably, was significantly higher and more confluent in long survivors given a combination of VP and RT + TMZ, compared to RT + TMZ alone (Figure 5C and D).

As the G-16302 PDX model was generated from an extremely aggressive and already recurrent patient tumor,[30] we performed additional VP survival studies using an orthotopic PDX model generated from primary (de novo) GBM. Indeed, in the more typical G-13063 PDX model, we detected significantly prolonged survival in mice treated with daily IP injections of VP as monotherapy, compared to VEH control mice (Figure 5E). Notably, 10 mg/kg daily IP injection of VP for 171-276 days was well tolerated by most mice, showing steady weight during the long course of drug treatment and weight loss corresponding to tumor formation (Supplementary Figure 6D), which we confirmed histologically. These results provide strong support that VP not only impedes invasive tumor cell behavior in vitro and in vivo but also confers survival benefits in preclinical PDX mouse models without associated systemic toxicity.

Discussion

New therapeutics that effectively target the infiltrative aspect of GBM growth are greatly needed to improve disease prognosis[5] and repurposing FDA-approved drugs for mono or combination therapies may prove effective in this endeavor.[39] The unique ability of Hippo to converge complex biochemical and mechanical signals onto transcriptional regulation makes the pathway's effector YAP-TEAD, a prime target for simultaneously inhibiting multiple aspects of the biology driving tumor proliferation, invasion, and migration. Here, we use the FDA-approved drug and small molecule YAP-TEAD inhibitor VP to target this convergence point for regulating tumor invasion/metastasis and establish the robust anti-invasive therapeutic efficacy of this drug across preclinical glioma models.

An emerging hypothesis in the field is that effective GBM therapy target both tumor cell proliferation and invasion, and our findings add to previous studies to support the role of VP as a combined anti-proliferative and anti-invasive drug agent. Several mechanisms of VP action have been previously reported to explain its observed efficacy in gliomas, related both to on-target Hippo activity[24] as well as to off-target cytotoxicity under hypoxia[25] and enhanced oxidative phosphorylation.[26] Here, we demonstrate the additional inhibitory effect of VP on tumor migration, invasion, and mesenchymal transition. VP treatment downregulated many EMT-associated genes, especially those involved in ECM assembly and adhesion. Interestingly, VP treatment consistently disrupted a treatment-resistant PMT signature in GBM cell lines, despite their unique molecular makeup. We believe this anti-mesenchymal/anti-invasive VP effect to be at least partially related to TEAD activity, as the observed inhibitory VP effects were phenocopied functionally[8] and molecularly (this study) after TEAD1 knockout in similar patient-derived lines. Moreover, genetic inhibition of TAZ-TEAD2 activity has previously shown similar anti-invasive phenotype and a mesenchymal-to-proneural switch in GBM[13] and both TEAD1 and YAP/TAZ have been described as critical upstream regulators of GSC cell fate, including for tumor initiation[8,40] and migration.[8] We confirmed VP-associated downregulation of the mesenchymal cadherin *CDH2* and the integrin *ITGB1* in vivo, two known pro-invasion glioma molecules[41,42] and YAP-TEAD-associated target genes,[8,43] in tumors with reduced infiltrative spread and decreased nuclear YAP and TEAD1 expression. VP also inhibited levels of EGFR in our tumors, a key oncogenic GBM driver.[44] This is consistent

Fig. 4, continued
serial histological sections per mouse, 4-wk pt and VEH/VP treatment and 3-wk pt with no treatment (NT) (*P = .0161; n = 11 mice (dots) per condition from 2 combined experiments, normalized to average VEH tumor burden area; similar results observed in 3 independent experiments). (C, D) Representative histological images (C) and quantifications (D) of Ki67 tumor core intensity normalized to HNA (10 mg/kg IP VP administration days 1-28; *P = .027; n = 6 (VP) and n = 4 (VEH)-treated G-16302 PDX mice (dots)). Scale bars = 100 µm. (E, F) Representative immunofluorescence images (E) and quantification (F) of CDH2 expression in VP/VEH-treated PDX tumors (10 mg/kg IP days 1-28 and 100 mg/kg IP days 21-30; *P = .0136; n = 4 G-16302 PDX mice (dots) per condition). Scale bars = 30 µm. (G, H) Representative images (G) and quantifications (H) of single migratory HNA+ tumor cells (annotated in yellow) away from the core and infiltrative edge in PDX mice with early Verteporfin treatment regimen (10 mg/kg IP days 1-28) (*P = .04; n = 6 G-16302 PDX mice (dots) per condition, section with largest tumor burden annotated for each). Scale bars = 1 mm. See also Supplementary Figure 5F. For parts B, D, F, and H, lines in box-and-whisker plots represent mean and bars represent min/max; P-values determined by Student t test. Abbreviations: IP, intraperitoneally; PDX, patient-derived orthotopic xenograft; VEH, vehicle; VP, Verteporfin.

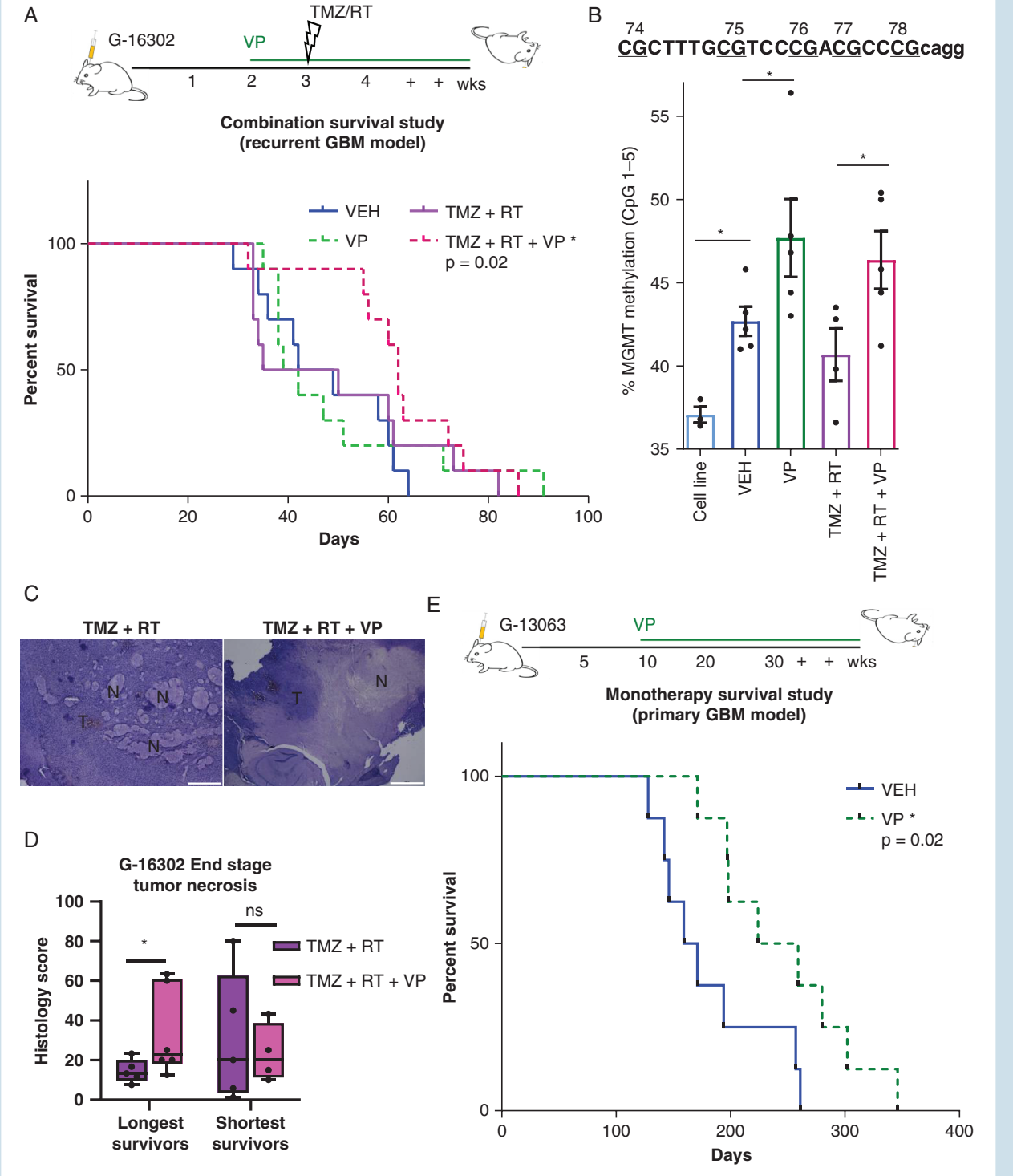

Fig. 5 Verteporfin survival studies in primary and recurrent GBM models. (A) Experimental setup (top) and Kaplan-Meier survival analysis (bottom) of Verteporfin treatment alone or in combination with standard chemoradiation therapy, Temozolomide plus Radiation (TMZ + RT) in the recurrent GBM G-16302 PDX model, gender-matched (VP = 10 mg/kg IP beginning on day 14, TMZ = 5 mg/kg days 21-22, two fractions of whole brain 3Gy RT days 21-22). Combined VP + TMZ + RT treatment confers survival benefit over vehicle (*P = .02 VP + TMZ + RT vs VEH; P = .72 VP vs VEH; P = .55 TMZ + RT vs VEH; P = .76 TMZ + RT vs VP; P = .26 VP + TMZ + RT vs VP; P = .23 VP + TMZ + RT vs TMZ + RT; chi-square log-rank test; n = 9 mice/treatment condition, median survival 45.5/40.5/42.5/62 days for VEH/VP/TMZ + RT/VP + TMZ + RT, respectively). (B) DNA methylation analysis of human *MGMT* comparing cell line (G-16302, n = 3 technical replicates (dots)) and the survival cohorts of G-16302 PDX tumors at end stage (n = 5 PDX mice (dots) per treatment group, *P < .05 by Student t test). (C) Representative hematoxylin and eosin (H&E) images of tumor necrosis in PDX tumors of TMZ + RT and TMZ + RT + VP-treated mice. Scale bar = 1 mm. T, tumor; N, necrosis. (D) Pathological scoring of percentage

with the recent discovery that *EGFR* is a direct TEAD-target gene in esophageal cancer[22] and in GBM,[8] and the subsequent demonstration of VP's therapeutic potential in lung cancer[45,46] and in EGFR-mutant GBM.[29] Our findings suggest widespread VP efficacy against IDH-wildtype GBM tumors, including EGFR-mutant, NF1-mutant, and/or PDGFRA-amplified subtypes.

Survival studies demonstrated a clear benefit of VP as monotherapy in the primary (de novo) G-13063 GBM model and suggested partial benefit of VP when combined with chemoradiation in the recurrent G-16302 GBM model, where statistically significant difference in survival was detected only when VP + TMZ + RT is compared to VEH treatment. While comparison between VP + TMZ + RT and TMZ + RT treatment groups did not reach statistical significance, we did observe a transient pro-survival effect in a subset of animals when VP is added to chemoradiation. Recent in vitro studies have shown additive efficacy of VP when combined with TMZ[27] or with radiation.[28,47] Consistent with this, our molecular analysis revealed higher levels of *MGMT* methylation in VP-treated G-16302 tumors, a clinically relevant biomarker for TMZ response, and a greater degree of treatment-related necrosis in long PDX survivors treated with VP plus chemoradiation. The exact mechanisms through which VP potentially induces TMZ chemosensitivity and/or radioresistance in recurrent GBM deserve focused investigation in future studies.

Overall, our data suggest that VP inhibits migration/invasion and mesenchymal transition across different GBM tumors, both primary and recurrent, which appears at least partially related to TEAD1-associated activity. This, in addition to VP's other effects on TMZ, radiotherapy, and cytotoxicity may prove this drug beneficial in simultaneously targeting migratory and proliferative biology in a diverse population of GBM tumors.

Prior pharmacokinetic studies have evaluated extensively the biodistribution of the active metabolite in VP, in several organs including the brain[37,48,49] and have shown much greater VP metabolite accumulation in tumors than in normal tissues.[38] Our study also revealed greater VP efficacy in dense tumor regions (tumor core and infiltrative edge) than in distal migratory cells within the mostly normal host parenchyma. Therefore, VP's greatest therapeutic efficacy is expected to be at the core and infiltrative edge, when given soon after tumor detection/resection, with the hope that decreasing collective migration at the margin will also deter further distal tumor cell spread. Unlike many small molecule inhibitors, the plant-derived drug VP has minimal toxicity to non-tumor cells and has been used for decades as porphyrin-based photosensitizer therapy. Several incidental case reports have also demonstrated the efficacy of VP in treating aggressive retinal astrocytic lesions, with little side effects.[50–52] In our study, we also observed drug efficacy in vivo in the absence of systemic toxicity, at VP doses ranging from 6 to 100 mg/kg, after up to 10 months of daily VP treatment. Given that VP is FDA-approved and well tolerated in patients for the treatment of macular generation and we have herein demonstrated a role for VP in prolonging survival in the absence of toxicity in both primary and recurrent GBM models, the drug's repurposing for use as adjuvant therapy in GBM patients should be strongly considered in future studies.

Supplementary Material

Supplementary material is available at *Neuro-Oncology* online.

Keywords

invasion | migration | preclinical | Verteporfin | YAP-TEAD

Funding

This study was supported by the National Institutes of Health (R01NS106229 to N.M.T., P30CA196521 to Tisch Cancer Institute, T32GM62754 to A.M.B.)

Acknowledgments

We thank members in Pathology, Neurosurgery, and ISMMS's Biorepository Core for facilitating tissue procurement and Yu Zhou at the ISMMS Imaging Core for help with IVIS.

Conflict of interest statement. The authors declare no competing interests.

Authorship statement. Conception of the project: N.M.T. Experimental design and data interpretation: N.M.T., A.M.B., M.R.B., C.G.H., and E.Z. Cell culture and functional assays, PDX, IC/IF, RNA work, image analysis: A.M.B., H.R., T.J., Z.M., and R.Y. IVIS and chemoradiation: A.M.B., A.B., J.G.R., and D.B. MGMT: M.M., W.L., T.J., N.T., and J.H. Bioinformatics: G.N., E.Z., Z.M., A.M.B., and N.T. Manuscript preparation: N.M.T. and A.M.B.; Editing: all authors.

Fig. 5, continued
necrosis stratified into 2 groups based on longest and shortest survival (n = 10 mice (dots) per treatment group, 2-4 sections per mouse, $*P < .05$ by Student *t* test, lines in box-and-whisker plots represent mean, bars represent min/max; ns, not significant). (E) Experimental setup (top) and Kaplan-Meier survival analysis (bottom) of Verteporfin vs vehicle treatment in G-13063 orthotopic PDX mice ($*P = .02$ by chi-square log-rank test; n = 9 mice/treatment condition, median survival 171/211 days for VEH/VP, respectively; tumors confirmed in all mice included in the analysis). Abbreviations: GBM, glioblastoma; PDX, patient-derived orthotopic xenograft; RT, radiation therapy; TMZ, Temozolomide; VEH, vehicle; VP, Verteporfin.

References

1. Brat DJ, Castellano-Sanchez AA, Hunter SB, et al. Pseudopalisades in glioblastoma are hypoxic, express extracellular matrix proteases, and are formed by an actively migrating cell population. *Cancer Res.* 2004;64(3):920–927.
2. Xie Q, Mittal S, Berens ME. Targeting adaptive glioblastoma: an overview of proliferation and invasion. *Neuro Oncol.* 2014;16(12):1575–1584.
3. Cooper LA, Gutman DA, Chisolm C, et al. The tumor microenvironment strongly impacts master transcriptional regulators and gene expression class of glioblastoma. *Am J Pathol.* 2012;180(5):2108–2119.
4. Darmanis S, Sloan SA, Croote D, et al. Single-cell RNA-seq analysis of infiltrating neoplastic cells at the migrating front of human glioblastoma. *Cell Rep.* 2017;21(5):1399–1410.
5. Zhong J, Paul A, Kellie SJ, Neill GMO. Mesenchymal migration as a therapeutic target in glioblastoma. *J Oncol.* 2010;2010:430142.
6. Lathia JD, Mack SC, Mulkearns-Hubert EE, Valentim CLL, Rich JN. Cancer stem cells in glioblastoma. *Genes Dev.* 2015;26(10):758.
7. Lan X, Jörg DJ, Cavalli FMG, et al. Fate mapping of human glioblastoma reveals an invariant stem cell hierarchy. *Nature.* 2017;549(7671):227–232.
8. Tome-Garcia J, Erfani P, Nudelman G, et al. Analysis of chromatin accessibility uncovers TEAD1 as a regulator of migration in human glioblastoma. *Nat Commun.* 2018;9(1):1–13.
9. Meng Z, Moroishi T, Guan KL. Mechanisms of Hippo pathway regulation. *Genes Dev.* 2016;30(1):1–17.
10. Li W, Dong S, Wei W, et al. The role of transcriptional coactivator TAZ in gliomas. *Oncotarget.* 2016;7(50):82686–82699.
11. Zhang H, Geng D, Gao J, et al. Expression and significance of Hippo/YAP signaling in glioma progression. *Tumor Biol.* 2016;37(12):15665–15676.
12. Artinian N, Cloninger C, Holmes B, Benavides-Serrato A, Bashir T, Gera J. Phosphorylation of the Hippo pathway component AMOTL2 by the mTORC2 kinase promotes YAP signaling, resulting in enhanced glioblastoma growth and invasiveness. *J Biol Chem.* 2015;290(32):19387–19401.
13. Bhat KP, Salazar KL, Balasubramaniyan V, et al. The transcriptional coactivator TAZ regulates mesenchymal differentiation in malignant glioma. *Genes Dev.* 2011;25(24):2594–2609.
14. Minata M, Audia A, Shi J, et al. Phenotypic plasticity of invasive edge glioma stem-like cells in response to ionizing radiation. *Cell Rep.* 2019;26(7):1893–1905.e7.
15. Nawaz Z, Patil V, Arora A, et al. Cbx7 is epigenetically silenced in glioblastoma and inhibits cell migration by targeting YAP/TAZ-dependent transcription. *Sci Rep.* 2016;6:1–14.
16. Yang R, Wu Y, Zou J, et al. The Hippo transducer TAZ promotes cell proliferation and tumor formation of glioblastoma cells through EGFR pathway. *Oncotarget.* 2016;5(24). doi:10.18632/oncotarget.9199.
17. Yu OM, Benitez JA, Plouffe SW, et al. YAP and MRTF-A, transcriptional co-activators of RhoA-mediated gene expression, are critical for glioblastoma tumorigenicity. *Oncogene.* 2018;37(41):5492–5507.
18. Zhang Y, Xie P, Wang X, et al. YAP promotes migration and invasion of human glioma cells. *J Mol Neurosci.* 2018;64(2):262–272.
19. Liu-Chittenden Y, Huang B, Shim JS, et al. Genetic and pharmacological disruption of the TEAD-YAP complex suppresses the oncogenic activity of YAP. *Genes Dev.* 2012;26(12):1300–1305.
20. Szeto SG, Narimatsu M, Lu M, et al. YAP/TAZ are mechanoregulators of TGF-β-Smad signaling and renal fibrogenesis. *J Am Soc Nephrol.* 2016;27(10):3117–3128.
21. Feng J, Gou J, Jia J, Yi T, Cui T, Li Z. Verteporfin, a suppressor of YAP-TEAD complex, presents promising antitumor properties on ovarian cancer. *Onco Targets Ther.* 2016;9:5371–5381.
22. Song S, Honjo S, Jin J, et al. The Hippo coactivator YAP1 mediates EGFR overexpression and confers chemoresistance in esophageal cancer. *Clin Cancer Res.* 2015;21(11):2580–2590.
23. Wei H, Wang F, Wang Y, et al. Verteporfin suppresses cell survival, angiogenesis and vasculogenic mimicry of pancreatic ductal adenocarcinoma via disrupting the YAP-TEAD complex. *Cancer Sci.* 2017;108(3):478–487.
24. Al-Moujahed A, Brodowska K, Stryjewski TP, et al. Verteporfin inhibits growth of human glioma in vitro without light activation. *Sci Rep.* 2017;7(1):7602.
25. Eales KL, Wilkinson EA, Cruickshank G, Tucker JHR, Tennant DA. Verteporfin selectively kills hypoxic glioma cells through iron-binding and increased production of reactive oxygen species. *Sci Rep.* 2018;8(1):1–12.
26. Kuramoto K, Yamamoto M, Suzuki S, et al. Verteporfin inhibits oxidative phosphorylation and induces cell death specifically in glioma stem cells. *FEBS J.* 2020;287(10):2023–2036.
27. Pellosi DS, Paula LB, de Melo MT, Tedesco AC. Targeted and synergic glioblastoma treatment: multifunctional nanoparticles delivering verteporfin as adjuvant therapy for temozolomide chemotherapy. *Mol Pharm.* 2019;16(3):1009–1024.
28. Shah SR, Kim J, Schiapparelli P, et al. Verteporfin-loaded polymeric microparticles for intratumoral treatment of brain cancer. *Mol Pharm.* 2019;16(4):1433–1443.
29. Vigneswaran K, Boyd NH, Oh SY, et al. YAP/TAZ transcriptional coactivators create therapeutic vulnerability to verteporfin in EGFR-mutant glioblastoma. *Clin Cancer Res.* 2021;27(5):1553–1569.
30. Umphlett M, Shea S, Tome-Garcia J, et al. Widely metastatic glioblastoma with BRCA1 and ARID1A mutations: a case report. *BMC Cancer.* 2020;20(1):1–8.
31. Tome-Garcia J, Tejero R, Nudelman G, et al. Prospective isolation and comparison of human germinal matrix and glioblastoma EGFR+ populations with stem cell properties. *Stem Cell Rep.* 2017;8(5):1421–1429.
32. Wang C, Zhu X, Feng W, et al. Verteporfin inhibits YAP function through up-regulating 14-3-3σ sequestering YAP in the cytoplasm. *Am J Cancer Res.* 2016;6(1):27–37.
33. Anastassiou D, Rumjantseva V, Cheng W, et al. Human cancer cells express Slug-based epithelial-mesenchymal transition gene expression signature obtained in vivo. *BMC Cancer.* 2011;11:529.
34. Segerman A, Niklasson M, Haglund C, et al. Clonal variation in drug and radiation response among glioma-initiating cells is linked to proneural-mesenchymal transition article clonal variation in drug and radiation response among glioma-initiating cells is linked to proneural-mesenchymal transition. *Cell Rep.* 2016:2994–3009.
35. Vinci M, Box C, Zimmermann M, Eccles SA. Tumor spheroid-based migration assays for evaluation of therapeutic agents. *Methods Mol Biol.* 2013;986:253–266.
36. Dundar B, Markwell SM, Sharma NV, Olson CL, Mukherjee S, Brat DJ. Methods for in vitro modeling of glioma invasion: choosing tools to meet the need. *Glia.* 2020;68(11):2173–2191.
37. Ziemssen F, Heimann H. Evaluation of verteporfin pharmacokinetics–redefining the need of photosensitizers in ophthalmology. *Expert Opin Drug Metab Toxicol.* 2012;8(8):1023–1041.
38. Richter AM, Cerruti-Sola S, Sternberg ED, Dolphin D, Levy JG. Biodistribution of tritiated benzoporphyrin derivative (3H-BPD-MA), a new potent photosensitizer, in normal and tumor-bearing mice. *J Photochem Photobiol B.* 1990;5(2):231–244.
39. Gupta SK, Kizilbash SH, Daniels DJ, Sarkaria JN. Editorial: targeted therapies for glioblastoma: a critical appraisal. *Front Oncol.* 2019;9:1–4.
40. Castellan M, Guarnieri A, Fujimura A, et al. Single-cell analyses reveal YAP/TAZ as regulators of stemness and cell plasticity in glioblastoma. *Nat Cancer.* 2020;2(2):174–188.

41. Edwards LA, Woolard K, Son MJ, et al. Effect of brain- and tumor-derived connective tissue growth factor on glioma invasion. *J Natl Cancer Inst.* 2011;103(15):1162–1178.
42. Kohutek ZA, Charles G, Redpath GT, Hussaini IM. ADAM-10-mediated N-cadherin cleavage is protein kinase C-α dependent and promotes glioblastoma cell migration. *J Neurosci.* 2009;29(14):4605–4615.
43. Nardone G, Oliver-De La Cruz J, Vrbsky J, et al. YAP regulates cell mechanics by controlling focal adhesion assembly. *Nat Commun.* 2017;8:15321.
44. Keller S, Schmidt MHH. EGFR and EGFRvIII promote angiogenesis and cell invasion in glioblastoma: combination therapies for an effective treatment. *Int J Mol Sci.* 2017;18(6):1–19.
45. Hsu PC, You B, Yang YL, et al. YAP promotes erlotinib resistance in human non-small cell lung cancer cells. *Oncotarget.* 2016;7(32):51922–51933.
46. Cheng H, Zhang Z, Rodriguez-Barrueco R, et al. Functional genomics screen identifies YAP1 as a key determinant to enhance treatment sensitivity in lung cancer cells. *Oncotarget.* 2016;7(20):28976–28988.
47. Zhang Y, Wang Y, Zhou D, et al. Radiation-induced YAP activation confers glioma radioresistance via promoting FGF2 transcription and DNA damage repair. *Oncogene.* 2021;40(27):4580–4591.
48. Richter AM, Waterfield E, Jain AK, et al. Photosensitising potency of structural analogues of benzoporphyrin derivative (BPD) in a mouse tumour model. *Br J Cancer.* 1991;63(1):87–93.
49. Zhou X, Pogue BW, Chen B, Hasan T. Analysis of effective molecular diffusion rates for verteporfin in subcutaneous versus orthotopic Dunning prostate tumors. *Photochem Photobiol.* 2004;79(4):323–331.
50. Eskelin S, Tommila P, Palosaari T, Kivelä T. Photodynamic therapy with verteporfin to induce regression of aggressive retinal astrocytomas. *Acta Ophthalmol.* 2008;86(7):794–799.
51. House RJ, Mashayekhi A, Shields JA, Shields CL. Total regression of acquired retinal astrocytoma using photodynamic therapy. *Retin Cases Brief Rep.* 2016;10(1):41–43.
52. Tuncer S, Cebeci Z. Dramatic regression of presumed acquired retinal astrocytoma with photodynamic therapy. *Middle East Afr J Ophthalmol.* 2014;21(3):283–286.